

QoS-Aware Hierarchical Reinforcement Learning for Joint Link Selection and Trajectory Optimization in SAGIN-Supported UAV Mobility Management

Jiayang Wan, *Graduate Student Member, IEEE*, Ke He, *Member, IEEE*,
 Yafei Wang, *Graduate Student Member, IEEE*, Fan Liu, *Senior Member, IEEE*,
 Wenjin Wang, *Member, IEEE*, Shi Jin, *Fellow, IEEE*

Abstract—Due to the significant variations in unmanned aerial vehicle (UAV) altitude and horizontal mobility, it becomes difficult for any single network to ensure continuous and reliable three-dimensional coverage. Towards that end, the space-air-ground integrated network (SAGIN) has emerged as an essential architecture for enabling ubiquitous UAV connectivity. To address the pronounced disparities in coverage and signal characteristics across heterogeneous networks, this paper formulates UAV mobility management in SAGIN as a constrained multi-objective joint optimization problem. The formulation couples discrete link selection with continuous trajectory optimization. Building on this, we propose a two-level multi-agent hierarchical deep reinforcement learning (HDRL) framework that decomposes the problem into two alternately solvable subproblems. To map complex link selection decisions into a compact discrete action space, we conceive a double deep Q-network (DDQN) algorithm in the top-level, which achieves stable and high-quality policy learning through double Q-value estimation. To handle the continuous trajectory action space while satisfying quality of service (QoS) constraints, we integrate the maximum-entropy mechanism of the soft actor-critic (SAC) and employ a Lagrangian-based constrained SAC (CSAC) algorithm in the lower-level that dynamically adjusts the Lagrange multipliers to balance constraint satisfaction and policy optimization. Moreover, the proposed algorithm can be extended to multi-UAV scenarios under the centralized training and decentralized execution (CTDE) paradigm, which enables more generalizable policies. Simulation results demonstrate that the proposed scheme substantially outperforms existing benchmarks in throughput, link switching frequency and QoS satisfaction.

Index Terms—SAGIN, UAV, trajectory optimization, link selection, QoS constraints, hierarchical deep reinforcement learning.

I. INTRODUCTION

With the rapid expansion of the low-altitude economy, existing terrestrial networks (TNs) [1] cannot ensure continuous and reliable coverage in low-altitude airspace characterized by significant altitude variations and high horizontal mobility, resulting in pronounced coverage gaps. To overcome this limitation, emerging non-terrestrial networks

Jiayang Wan, Yafei Wang, and Wenjin Wang are with the National Mobile Communications Research Laboratory, Southeast University, Nanjing 210096, China, and also with Purple Mountain Laboratories, Nanjing 211100, China (e-mail: {jywan, wangyf, wangwj}@seu.edu.cn).

K. He is with the Interdisciplinary Centre for Security, Reliability and Trust (SnT), University of Luxembourg, L-1855 Luxembourg, Luxembourg (e-mail: ke.he@ieee.org).

F. Liu and S. Jin are with the National Mobile Communications Research Laboratory, Southeast University, Nanjing 210096, China (e-mail: {fan.liu, jinshi}@seu.edu.cn).

(TNs), such as low-altitude wireless networks (LAWNs) and satellite communication systems [2], [3], serve as effective complements by providing wide-area connectivity in regions beyond the coverage of TNs. Consequently, the space-air-ground integrated network (SAGIN) [4], [5], which integrates TNs with LAWNs and satellite communication networks, has emerged as a key architecture for enabling wide-area and seamless connectivity in low-altitude airspace [6], [7].

In SAGIN, unmanned aerial vehicles (UAVs), as a new class of aerial users, are increasingly deployed in mission-critical applications such as environmental monitoring, aerial imaging, air transportation, and disaster relief [8]. During operation, UAVs must simultaneously perform link selection and trajectory optimization. However, due to the coexistence of heterogeneous networks with diverse coverage, frequent link switching is triggered, resulting in excessive overhead and unstable connectivity [9]. Moreover, since the distinct link dynamics between TNs and TNs, where TN links vary rapidly with propagation distance while NTN links remain relatively stable, UAV trajectory optimization becomes particularly challenging [10].

A. Prior Work

Owing to significant variations in UAV altitude and high horizontal mobility, UAVs frequently traverse ground, aerial, and satellite coverage regions, making link selection a key research problem in UAV communications. Depending on whether the decision is made within a single network or across multiple networks, link selection can be classified into two categories: intra-network link selection [11]–[18] and inter-network link selection [19]–[21]. Intra-network link selection primarily concerns UAV associations among nodes within the same network type. In TNs, a UAV switches its link between ground base stations (GBSs) when a target GBS provides better channel quality than the serving GBS. To reduce link switching frequency, link selection triggering is regulated via control parameters such as hysteresis, time-to-trigger (TTT), and cell individual offset (CIO) [11], [12]. As emphasized in [13], efficient connectivity management is crucial for mobile nodes within the network, such as UAVs and trains. The authors in [14] investigate a deep reinforcement learning (DRL)-based connectivity management scheme to dynamically adjust link selection decisions. In [15], the authors study machine learning-based link selection prediction and demon-

strate significant improvements in communication efficiency and reliability. In contrast, connectivity management in NTNs exhibits relatively smooth link dynamics, where conventional TN-based criteria may trigger unnecessary link switching and excessive overhead [16]–[18]. To address this issue, NTN-specific strategies have been proposed that incorporate satellite positions and predictable orbital information into link selection conditions, thereby reducing link switching frequency [16]. In addition, several studies have proposed multi-metric optimization approaches that jointly optimize resource allocation and traffic offloading to enhance NTN service capability [17]. Moreover, a conditional handover (CHO)-based optimization strategy is proposed in [18] for low Earth orbit (LEO) satellite networks, where a service continuity model is leveraged to effectively reduce link switching frequency.

When it comes to inter-network link selection, the substantial differences in signal characteristics and coverage footprints between TNs and NTNs render link selection more complex than its intra-network counterpart [19]–[21]. A cross-level link selection model based on stochastic geometry is developed in [19], and closed-form expressions for key performance metrics, such as the link switching rate, failure rate, and ping-pong rate, are derived. In [20], TN-NTN cross-domain link selection mechanisms are examined, and it is demonstrated that effective inter-network coordination can enhance resource utilization for remote users. In addition, a graph-based UAV mobility management strategy is proposed in [21], where TNs and NTNs are treated as both competitive and cooperative network entities, and the inter-network link selection process is dynamically optimized to improve communication continuity while reducing link switching frequency. However, these studies, while focusing on link selection optimization in heterogeneous networks, do not adequately account for UAV trajectory optimization, which significantly affects both link selection frequency and stability.

As a key enabling technique for UAV communication systems, trajectory optimization plays a critical role in enhancing communication performance and mission efficiency through intelligent flight path planning [22]–[29]. Existing optimization- and heuristic-based approaches [22]–[24] mainly include graph-theoretic methods [22], convex optimization [23], and dynamic programming (DP) [24]. Specifically, [22] develops a trajectory design framework that integrates graph theory with convex optimization, with the objective of minimizing the UAV's flight time while maintaining continuous connectivity with at least one GBS. Building upon this line of research, [24] adopts a dynamic programming (DP) approach to generate UAV trajectories that effectively constrain the duration of disconnection from GBSs during task execution. In addition, [23] incorporates communication outage constraints into a graph-theoretic optimization framework to jointly optimize UAV trajectory and link reliability. However, these methods are inherently designed for single-stage or short-horizon objectives and fail to capture long-term cumulative performance, rendering them less effective in complex and dynamic communication scenarios.

To address the limitations of optimization methods in dynamic environments, RL-based methods, especially DRL

[25]–[29], have received increasing attention. In particular, [25] proposed a DRL-based coverage-aware navigation framework for cellular-connected UAVs to minimize mission time and communication outage, while [26] employed a deep Q-network (DQN)-based scheme to jointly optimize mission duration, trajectory, and BS association for energy-efficient and reliable connectivity. An RL-based framework is developed in [27], [28] to dynamically adjust the CIO of aerial and ground BSs, thereby maximizing user capacity while reducing link selection failures and ping-pong effects. To minimize the frequency of link switching, [29] optimizes UAV trajectories with a graph theory-based approach under communication and mission constraints. The aforementioned methods discretize the continuous trajectory action space of UAVs to simplify learning and decision-making, which limits fine-grained modeling of continuous motion and hinders the full potential of trajectory optimization. Moreover, these studies typically select the link with the maximum reference signal received power (RSRP) or signal-to-interference-plus-noise ratio (SINR), which can lead to high link switching frequency in heterogeneous network.

B. Motivation and Main Contributions

Although significant progress has been made in UAV trajectory optimization and link selection, the joint optimization of these two aspects for UAVs in SAGIN still faces two major challenges. First, the distinct signal characteristics across heterogeneous networks render conventional optimization methods less effective, necessitating novel algorithmic designs. Second, the strong coupling between discrete link selection and continuous trajectory optimization significantly increases the complexity of the joint optimization problem. Moreover, most existing works discretize the continuous trajectory action space, which limits fine-grained modeling of UAV motion, and employ greedy RSRP/SINR-based link selection strategies, leading to high link switching frequency.

Motivated by the above challenges, this paper formulates the joint link selection and trajectory optimization problem for UAVs in SAGIN as a constrained multi-objective optimization problem. The objective is to maximize the overall system throughput while minimizing the link switching frequency and UAV flight time, subject to communication quality-of-service (QoS) constraints. The main contributions of this work are summarized as follows:

- To efficiently address the strong coupling between discrete link selection variables and continuous trajectory optimization variables, we propose a two-level multi-agent hierarchical deep reinforcement learning (HDRL) framework [30] for joint link selection and trajectory optimization. The proposed framework decomposes the original problem into two subproblems that are solved in an alternating manner. In the top-level, the UAV-BS association indicator is updated to determine the serving BS, based on which the lower level further optimizes UAV trajectory control. Unlike conventional offline optimization methods, the proposed HDRL framework can be extended to multi-UAV scenarios under the centralized

training and decentralized execution (CTDE) paradigm, facilitating stable and generalizable policy learning.

- In the top-level, to compactly represent complex UAV-BS association decisions, we employ a double deep Q-network (DDQN) that maps the hybrid association space to two semantic actions: *Remain* and *Switch*. By leveraging double Q-value estimation to decouple action selection from action evaluation, the top-level agent effectively suppresses overestimation bias and achieves stable and fast-converging UAV-BS association policies.
- In the lower-level, to avoid performance degradation caused by discretizing the UAV’s continuous trajectory action space, we model trajectory control in a continuous action space. However, under this formulation, UAVs must simultaneously satisfy QoS constraints, which leads to complex nonlinear coupling between the state and decision variables. To tackle this challenge, we introduce a Lagrangian-based constrained soft actor-critic (CSAC) framework based on the principles of constrained reinforcement learning (CRL). This framework not only incorporates the maximum-entropy policy of SAC to enhance exploration and training stability, but also explicitly embeds constraint terms into the standard RL objective. As a result, the agent can maximize long-term cumulative rewards while dynamically adjusting the Lagrange multipliers to satisfy constraints, thereby avoiding tedious reward shaping and hyperparameter tuning.

Organization: The remainder of this paper is organized as follows. Section II presents the system model for UAVs in SAGIN. Section III formulates the joint UAV link selection and trajectory optimization problem. Section IV presents the proposed HDRL-based algorithm. Section V presents the simulation results, and Section VI concludes the paper.

Notation: Throughout this paper, bold uppercase letters denote matrices, and bold lowercase letters denote vectors. The operators $(\cdot)^T$, $(\cdot)^*$, and $(\cdot)^H$ represent the transpose, complex conjugate, and conjugate transpose, respectively. The function $\delta(\cdot)$ denotes the Dirac delta, which is widely used in signal processing, while $\|\cdot\|_F$ and $\|\cdot\|_2$ denote the Frobenius norm and the ℓ_2 norm, respectively.

II. SYSTEM MODEL

In this section, we first present the overall SAGIN architecture in Section II-A. Then, the signal model is described in detail in Section II-B. Subsequently, the UAV trajectory model and the link selection model are introduced in Sections II-C and II-D, which lay the foundation for problem formulation.

A. SAGIN Architecture

The considered SAGIN architecture is illustrated in Fig. 1 and consists of the following elements.

1) *Ground Network (GN):* The ground segment comprises multiple communication systems, including but not limited to cellular networks and wireless local area networks (WLANs) [31]. In this paper, we consider a ground cellular network consisting of G terrestrial cellular cells. Each cell is served by a GBS site with three co-located BSs, denoted by $b^{\text{GN}} \in \mathcal{B}^{\text{GN}}$, each covering a 120° sector [32].

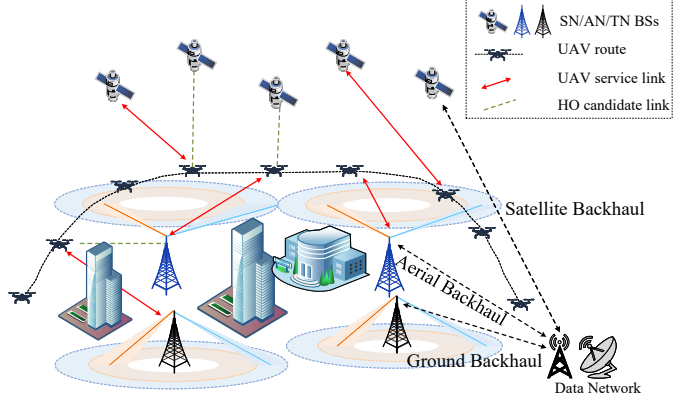


Fig. 1. Illustration of UAV trajectory and link selection in a SAGIN.

2) *Air Network (AN):* The aerial segment consists of UAVs, airships, balloon platforms, and exclusive-service aerial base stations (ABSs) for aerial users [33], which collectively form LAWNs. In this paper, we consider a low-altitude network consisting of L aerial cells. Each low-altitude cell is covered by one ABS site hosting three co-located BSs, denoted by $b^{\text{AN}} \in \mathcal{B}^{\text{AN}}$. Each ABS employs an independently designed antenna tilt angle to ensure reliable and efficient communications in the low-altitude region [33].

3) *Space Network (SN):* The space segment primarily comprises satellites operating at different altitudes and orbital configurations. In this paper, we consider a space network consisting of S low Earth orbit (LEO) satellites, collectively denoted by \mathcal{B}^{SN} . Each satellite is equipped with multiple beams whose pointing directions remain fixed with respect to the satellite body.

4) *Gateway & UAVs:* A gateway station integrates the service-area gateways of the ground, air, and space networks, establishing connections with all three network segments to facilitate content delivery from the Internet. Meanwhile, a swarm of UAVs performs flight missions in the low-altitude region, flying at certain speeds and requiring continuous link selection and trajectory optimization to maintain seamless connectivity and enable data reception in SAGIN. In what follows, we consider three types of links:

- *GN-UAV links*, connecting a GBS b^{GN} and a UAV u .
- *SN-UAV links*, connecting a satellite b^{SN} and a UAV u .
- *AN-UAV links*, connecting a ABS b^{AN} and a UAV u .

For GN-UAV and AN-UAV links, all BSs are assumed to be deployed at the same altitude, such that each BS provides coverage over a specific service area accessible to UAVs. For SN-UAV links, owing to the rapid movement of LEO satellites, we consider S LEO satellites to ensure continuous coverage along the UAV flight trajectory, thereby guaranteeing that at each time instant at least one satellite maintains connectivity with the UAV. In this work, we assume that each UAV can be connected to only one BS at a time.

B. Signal Model

Let $h_{b,u}(t)$ denote the baseband-equivalent channel between the b -th BS and the u -th UAV at time t , where $b \in \mathcal{B}$. The BS set \mathcal{B} is defined as $\mathcal{B} = \mathcal{B}^{\text{GN}} \cup \mathcal{B}^{\text{AN}} \cup \mathcal{B}^{\text{SN}}$, with $|\mathcal{B}| = B$. Accordingly, the received signal power at time t by the u -th UAV from the b -th BS is expressed as

$$\begin{aligned} p_{b,u}(t) &= \bar{P}_b |h_{b,u}(t)|^2 \\ &= \bar{P}_b \beta_{b,u}(\mathbf{q}_u(t)) G_{b,u}(\mathbf{q}_u(t)) \tilde{h}_{b,u}(t), \quad b = 1, \dots, B, \end{aligned} \quad (1)$$

where \bar{P}_b denotes the transmit power of the b -th BS, and $\beta_{b,u}(\cdot)$ and $G_{b,u}(\cdot)$ denote the large-scale channel gain and the BS antenna gain, respectively, both of which depend on the UAV location $\mathbf{q}_u(t)$. The term $\tilde{h}_{b,u}(t)$ is a random variable accounting for small-scale fading. It is worth noting that the proposed method is based on a model-free DRL framework and is therefore applicable to various antenna configurations and channel models.

We assume that the three networks operate over orthogonal frequency bands with distinct nominal carrier frequencies, such that inter-network interference can be neglected. This assumption allows us to focus on the variations in service capability across different networks induced by the mobility of satellites and UAVs. Considering the downlink transmission, the SINR of the u -th UAV served by the b -th BS is given by

$$\rho_u^{\text{GN}}(t) = \frac{\bar{P}_b |h_{b,u}(t)|^2}{\sum_{j \in \mathcal{B}^{\text{GN}} \setminus b} \bar{P}_j |h_{j,u}(t)|^2 + \sigma_{\text{GN}}^2}, \quad (2)$$

$$\rho_u^{\text{SN}}(t) = \frac{\bar{P}_b |h_{b,u}(t)|^2}{\sum_{j \in \mathcal{B}^{\text{SN}} \setminus b} \bar{P}_j |h_{j,u}(t)|^2 + \sigma_{\text{SN}}^2}, \quad (3)$$

$$\rho_u^{\text{AN}}(t) = \frac{\bar{P}_b |h_{b,u}(t)|^2}{\sum_{j \in \mathcal{B}^{\text{AN}} \setminus b} \bar{P}_j |h_{j,u}(t)|^2 + \sigma_{\text{AN}}^2}, \quad (4)$$

where σ^2 denotes the thermal noise variance at the u -th UAV under different network connections. The achievable rate $\mathcal{R}_u(t)$ of the b -th BS (either in GN, SN or AN) to the u -th UAV can be computed as

$$\mathcal{R}_u(t) = B_u \cdot \mathbb{E}[\log_2(1 + \rho_u(t))], \quad (5)$$

where the expectation is taken with respect to the small-scale fading, and B_u denotes the bandwidth allocated to the u -th UAV by its serving BS. Moreover, throughout the flight, each UAV occupies only one physical resource block (PRB) within a given network type, and multiple UAVs are assigned mutually orthogonal time-frequency resources.

C. UAV Trajectory Model

Without loss of generality, we consider a three-dimensional airspace specified by $[x_L, x_U] \times [y_L, y_U] \times [z_L, z_U]$. Each UAV flies from a random initial location $\mathbf{q}_u \in \mathbb{R}^{3 \times 1}$ to a common final location $\mathbf{q}_f \in \mathbb{R}^{3 \times 1}$. This setting applies to scenarios such as parcel collection or aerial inspection [34]. Multiple UAVs operate in the same airspace and share the destination \mathbf{q}_f , such that their flight experiences can be jointly leveraged to learn coverage-aware navigation policies maintained at the network side. For the considered SAGIN system, let T denote the mission completion time, and let $\mathbf{q}_u(t) \in \mathbb{R}^{3 \times 1}$, $t \in [0, T]$, denote the position of the u -th UAV. Accordingly, the following holds:

$$\begin{aligned} \mathbf{q}_u(0) &= \mathbf{q}_u, \quad \mathbf{q}_u(T) = \mathbf{q}_f, \\ \mathbf{q}_L \preceq \mathbf{q}_u(t) \preceq \mathbf{q}_U, \quad \forall t \in (0, T), \end{aligned} \quad (7)$$

where $\mathbf{q}_L \triangleq [x_L; y_L; z_L]$ and $\mathbf{q}_U \triangleq [x_U; y_U; z_U]$, with \preceq denoting the element-wise inequality.

D. UAV Link Selection Model

In TNs, UAV link selection mainly depends on rapid channel quality variations with propagation distance [10], whereas in satellite networks, link quality varies slowly due to the high orbital altitude, leading to distinct link selection evaluation criteria [35]. Consequently, when candidate BSs belong to different networks, a unified evaluation framework is required to accommodate the diverse temporal characteristics of their signal dynamics.

Greedy switching to the BS with the highest SINR may lead to an excessively high link switching frequency. To evaluate the service quality experienced by UAVs during flight, we focus on two key metrics: (i) the link rate $\mathcal{R}_u(t)$, which represents the achievable throughput between the UAV and the serving BS; and (ii) the number of link switches N_u , which characterizes the link switching frequency over the mission duration. Building on this, we introduce a UAV-BS association indicator $b_u(t)$, which denotes the index of the BS serving the u -th UAV at time t . A link switching event occurs when $b_u(t)$ changes, and the total number of link switches over the mission duration is defined as

$$N_u = \sum_{t \in (0, T]} \mathbf{1}\{b_u(t^-) \neq b_u(t)\}, \quad (8)$$

where $b_u(t^-)$ denotes the left-hand limit of $b_u(t)$ at time t , and $\mathbf{1}\{\cdot\}$ denotes the indicator function, which equals one if the condition inside the braces holds, and zero otherwise. This definition captures all discrete link switching events over the continuous-time domain. Therefore, we jointly employ $\mathcal{R}_u(t)$ and N_u to evaluate the service quality of UAV communications, enabling a unified assessment of candidate BSs.

III. PROBLEM FORMULATION AND TRANSFORMATION

A. Problem Formulation

In the considered SAGIN system, the objective is to maximize the average link rate of UAVs during flight while minimizing the link switching frequency and flight time, subject to communication QoS constraints. Accordingly, the optimization problem¹ is formulated as

$$\mathcal{P}_0 : \max_{\{\mathbf{q}(t), b(t)\}} \sum_{u \in \mathcal{U}} \left\{ \lambda_1 \frac{1}{T} \int_0^T \mathcal{R}_u(t) dt - \lambda_2 N_u - \lambda_3 T_u \right\}, \quad (9)$$

$$\text{s.t. } b_u(t) \in \{1, \dots, B\}, \quad \forall u, \quad (10)$$

$$\frac{1}{T} \int_0^T \mathcal{R}_u(t) dt > \mathcal{R}_{\text{req}}, \quad \forall u, \quad (11)$$

$$\mathbf{q}_u(0) = \mathbf{q}_u, \quad \mathbf{q}_u(T) = \mathbf{q}_f, \quad \forall u, \quad (12)$$

$$\mathbf{q}_L \preceq \mathbf{q}_u(t) \preceq \mathbf{q}_U, \quad \forall t \in [0, T], \forall u, \quad (13)$$

$$\vec{\mathbf{v}}_u(t) \cdot \vec{x} > 0, \quad \vec{x} = \mathbf{q}_{uf}, \quad \forall t \in [0, T], \forall u, \quad (14)$$

$$\|\dot{\mathbf{q}}_u(t)\| \leq V_{\text{max}}, \quad \forall t \in [0, T], \forall u, \quad (15)$$

where λ_1 , λ_2 , and λ_3 are weighting coefficients that trade off throughput enhancement, link switching frequency reduction, and flight time minimization, respectively. \mathcal{R}_{req} denotes the

¹The switching frequency is characterized by the number of changes in $b_u(t)$ over time. Since $b_u(t)$ is determined by the received SINR, which is a function of the UAV trajectory $\mathbf{q}(t)$, the switching frequency is implicitly determined by $\mathbf{q}(t)$.

minimum QoS rate requirement, $|\dot{\mathbf{q}}_u(t)|$ represents the instantaneous speed of the u -th UAV, V_{\max} denotes the maximum UAV speed, and T_u denotes the total flight time of the u -th UAV. In \mathcal{P}_0 , $b_u(t)$ represents the UAV-BS association, while $\mathbf{q}_u(t)$ denotes the UAV position; both jointly determine the SINR and the achievable rate of each link. Constraint (11) guarantees that each UAV maintains a service rate no lower than the minimum QoS requirement throughout the flight. Constraints (12) and (13) specify the trajectory boundary conditions, while constraint (14) imposes a directional velocity constraint, ensuring that the UAV continuously moves toward the destination. It can be shown that, with the optimal solution to \mathcal{P}_0 , UAVs should fly at the maximum speed V_{\max} , i.e., $\dot{\mathbf{q}}_u(t) = V_{\max} \vec{\mathbf{v}}_u(t)$, where $\vec{\mathbf{v}}_u(t)$ denotes the UAV flying direction vector with $\|\vec{\mathbf{v}}_u(t)\| = 1$. Thus, \mathcal{P}_0 is expressed as

$$\mathcal{P}_1 : \max_{\{\mathbf{q}(t), b(t), \vec{\mathbf{v}}(t)\}} \sum_{u \in \mathcal{U}} \left\{ \lambda_1 \frac{1}{T} \int_0^T \mathcal{R}_u(t) dt - \lambda_2 N_u - \lambda_3 T_u \right\}, \quad (16)$$

s.t. Constraints (10)–(14), (17)

$$\dot{\mathbf{q}}_u(t) = V_{\max} \vec{\mathbf{v}}_u(t), \quad \forall t \in [0, T], \forall u, \quad (18)$$

$$\|\vec{\mathbf{v}}_u(t)\| = 1, \quad \forall t \in [0, T], \forall u. \quad (19)$$

It can be observed that optimization problem \mathcal{P}_1 is a mixed-integer nonlinear programming (MINLP) problem formulated in continuous time, which is generally intractable. Moreover, in high-mobility scenarios, link switching and trajectory control must be performed in real time. Hence, due to the inherent non-convexity of the problem and the requirement for continuous-time optimization over the entire mission duration, traditional mathematical methods, such as convex optimization and game theory, are not well suited for this problem. To address these challenges, we propose a DRL-based approach that enables efficient online decision-making with low inference complexity after offline training.

B. Problem Transformation

The first step in applying RL algorithms to a real-world problem is to reformulate it as a Markov decision process (MDP). Since an MDP is defined over discrete time steps, for the joint link selection and trajectory optimization problem \mathcal{P}_1 , we discretize the time horizon $[0, T]$ into N time steps with a time interval Δt , where $T = N\Delta t$. Δt is properly chosen such that, within each time step, the large-scale channel gain and the BS antenna gain toward the UAV, i.e., $\beta_{b,u}(\mathbf{q}_u(t))$ and $G_{b,u}(\mathbf{q}_u(t))$ in (1), remain approximately constant. Accordingly, the continuous UAV trajectory $\{\mathbf{q}_u(t)\}$ can be approximated by a discrete sequence $\{\mathbf{q}_u(n)\}_{n=1}^N$, and the UAV position is given by

$$\mathbf{q}_u(n+1) = \mathbf{q}_u(n) + \Delta_s \vec{\mathbf{v}}_u(n), \quad \forall n, \quad (20)$$

where $\Delta_s = V_{\max} \Delta t$ denotes the UAV displacement per time step, and $\vec{\mathbf{v}}_u(n) \triangleq \vec{\mathbf{v}}(n\Delta t)$ represents the discretized flight direction vector of the u -th UAV at the n -th time step. Furthermore, since UAV-BS association is typically determined based on large-scale channel gains to avoid excessively frequent link switching, the associated BS is assumed to remain unchanged within each time step. Accordingly, the association indicator

$b_u(t)$ can be represented in discrete time as $b_u(n)$. As a result, the received signal power at the u -th UAV from the b -th BS in (1) can be rewritten as

$$\begin{aligned} p_{b,u}(n) &= \bar{P}_b |\mathbf{h}_{b,u}(n)|^2 \\ &= \bar{P}_b \beta_{b,u}(\mathbf{q}_u(n)) G_{b,u}(\mathbf{q}_u(n)) \tilde{h}_{b,u}(n), \end{aligned} \quad (21)$$

where $\mathbf{h}_{b,u}(n)$ denotes the baseband-equivalent channel between the b -th BS and the u -th UAV at the n -th time step. The term $p_{b,u}(n)$ represents the received signal power, and $\tilde{h}_{b,u}(n)$ is a random variable accounting for small-scale fading. At discrete time step n , given that the u -th UAV is associated with the b -th BS, the corresponding SINR is denoted by $\rho_u(n)$, and the achievable rate can be expressed as

$$\mathcal{R}_u(n) = B_u \cdot \mathbb{E}[\log_2(1 + \rho_u(n))]. \quad (22)$$

Accordingly, the total number of link switches defined in (8) can be approximated as

$$N_u \triangleq \sum_{n=2}^N \mathbf{1}\{b_u(n) \neq b_u(n-1)\}. \quad (23)$$

Based on the above discussion, \mathcal{P}_1 can be approximated as

$$\mathcal{P}_2 : \max_{\{\mathbf{q}(n), \vec{\mathbf{v}}(n), b(n)\}} \sum_{u \in \mathcal{U}} \left\{ \lambda_1 \frac{1}{N} \sum_{n=1}^N \mathcal{R}_u(n) - \lambda_2 N_u - \lambda_3 T_u \right\}, \quad (24)$$

s.t. $b_u(n) \in \{1, \dots, B\}, \quad \forall n, u,$ (25)

$$\mathbf{q}_u(n+1) = \mathbf{q}_u(n) + \Delta_s \vec{\mathbf{v}}_u(n), \quad \forall n, u, \quad (26)$$

$$\frac{1}{N} \sum_{n=1}^N \mathcal{R}_u(n) \geq \mathcal{R}_{\text{req}}, \quad \forall u, \quad (27)$$

$$\mathbf{q}_L \preceq \mathbf{q}_u(n) \preceq \mathbf{q}_U, \quad \forall n, u, \quad (28)$$

$$\mathbf{q}(0) = \mathbf{q}_u, \quad \mathbf{q}(N) = \mathbf{q}_f, \quad u, \quad (29)$$

$$\vec{\mathbf{v}}_u(n) \cdot \vec{x} > 0, \quad \vec{x} = \mathbf{q}_{uf}, \quad \forall n, u, \quad (30)$$

$$\|\vec{\mathbf{v}}_u(n)\| = 1, \quad \forall n, u. \quad (31)$$

It can be observed that problem \mathcal{P}_2 involves a hybrid action space with two types of decision variables: the discrete UAV-BS association indicator $b_u(n)$ and the continuous UAV trajectory $\mathbf{q}(n)$. Moreover, these two decision variables are strongly coupled and highly intertwined. Such a large hybrid action space significantly increases the decision-making complexity and may destabilize the learning process, rendering conventional DRL methods not well suited for this joint decision-making task.

IV. PROPOSED HDRL ALGORITHM

A. HDRL Framework

To address the challenges arising from the large hybrid action space and the strong coupling between discrete and continuous decision variables, we propose an HDRL framework composed of hierarchically organized DRL modules operating at different time scales. The proposed framework operates over two hierarchical levels: (i) a top-level module, described in Section IV-B, which takes the system state as input and determines the UAV-BS association; and (ii) a lower-level module, presented in Section IV-C, which leverages both the system state and the selected BS association to generate

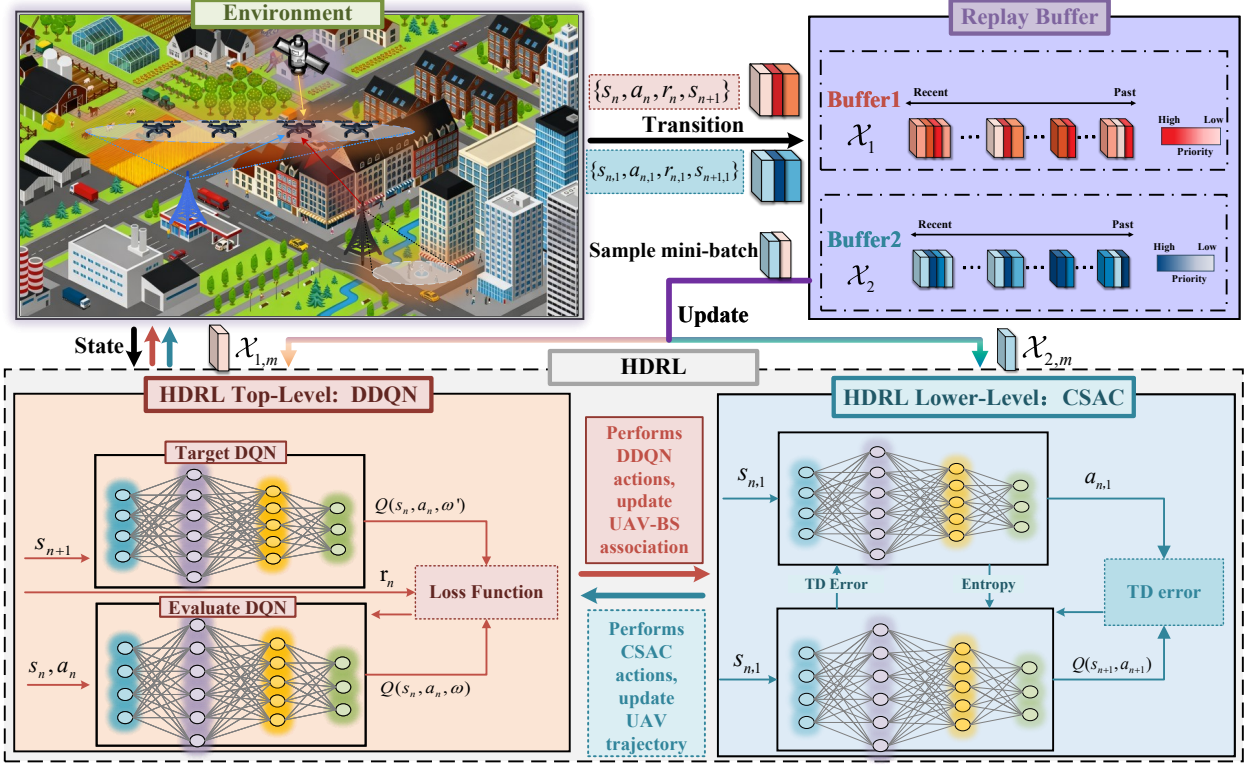


Fig. 2. The framework of the proposed HDRL algorithm for solving joint optimization of link selection and trajectory control.

continuous UAV trajectory actions until the current association terminates. Once the association expires, the top-level module selects a new BS association, and the above two-level decision-making process is repeated. The framework is trained using gradient-based optimization at different temporal scales, where the lower-level and top-level modules are optimized with respect to intrinsic rewards (Section IV-C) and extrinsic rewards (Section IV-B), respectively.

As illustrated in Fig. 2, the proposed HDRL framework consists of three main components: the environment, the replay buffer, and the HDRL network. The environment provides the UAVs with the current system state and returns the corresponding reward signal after each executed action. The HDRL network comprises a top-level DDQN, which outputs UAV-BS association decisions, and a lower-level CSAC, which generates continuous trajectory control actions; the resulting interaction data are then fed back to the environment. The replay buffer categorizes and stores the transition samples generated by the two hierarchical levels and supplies them for policy updates, thereby forming a closed-loop learning process. Details of the DDQN and CSAC designs are provided in Sections IV-B and IV-C, respectively, while the overall HDRL algorithm is presented in Section IV-D.

B. HDRL Top-Level: DDQN for UAV-BS Association

Unlike terrestrial networks, the heterogeneous architecture of SAGIN, characterized by diverse coverage patterns, renders UAV-BS association decisions highly complex, making the direct application of DRL difficult to train and prone to slow convergence. To address this issue, we design a DDQN-based top-level agent that maps the hybrid association space into only two semantic actions: *Remain* and *Switch*. By leveraging

double Q-value estimation to decouple action selection from action evaluation, the top-level agent effectively suppresses overestimation bias and achieves stable and fast-converging UAV-BS association policies. The state space, action space, reward function, and the DDQN algorithm are defined sequentially as follows.

1) *Top-Level State Space*: The state of the UAV at the n -th time step, denoted by s_n , consists of three components. The first component is the UAV-BS association indicator b_n , where $b_n = b \in \mathcal{B}$ denotes the index of the serving BS. The second component is the link rate between the UAV and its associated BS at the n -th time step, denoted by R_n . The third component is the UAV position $\mathbf{q}_n = (x_n, y_n, z_n)$. Accordingly, the state s_n is given by

$$s_n \triangleq [b_n, R_n, \mathbf{q}_n]^T. \quad (32)$$

2) *Top-Level Action Space*: To avoid action space expansion, non-stationarity, and unstable training caused by exhaustively considering all BSs, we model each UAV as an agent with two types of actions: *Remain*, which maintains the current association, and *Switch*, which updates the association to the candidate BS with the highest state-action value (Q-value). Specifically, the action $a_n \in \mathcal{A}$ can be denoted by

$$a_n = \{\text{Remain}, \text{Switch}\}, \quad (33)$$

After executing action a_n , the UAV-BS association indicator is updated from the previous connection state b_n to b_{n+1} . If $b_{n+1} = b_n$, the UAV maintains its connection to the same BS; otherwise, the UAV switches to a new BS. In the top-level decision process, the designed state space retains only the three most relevant elements for UAV-BS association, thereby achieving a minimally sufficient representation for link selection. Meanwhile, the original action space over

numerous candidate BSs is compressed into a binary set, which substantially reduces the complexity of the top-level decision-making.

3) *Top-Level Reward Function*: To encourage the UAV to maintain a high link rate throughout its mission (24), the rate reward r_n^R is defined as

$$r_n^R = (R_{n+1} - \min_E\{R\}) / (\max_E\{R\} - \min_E\{R\}), \quad (34)$$

where R_{n+1} denotes the link rate of UAV after executing action a_n and transitioning to the next state s_{n+1} . The terms $\max_E\{R\}$ and $\min_E\{R\}$ represent the maximum and minimum link rates, respectively. To reduce the link switching frequency in (24), a penalty r_n^M is introduced as

$$r_n^M = \begin{cases} 0, & \text{if } b_{n+1} = b_n, \\ -1, & \text{if } b_{n+1} \neq b_n. \end{cases} \quad (35)$$

Therefore, the overall extrinsic reward consists of two components: a rate reward and a link switching penalty, which can be expressed as

$$r_n(s_n, a_n) = \lambda_1 \cdot r_n^R + \lambda_2 \cdot r_n^M, \quad (36)$$

where λ_1 and λ_2 are weighting factors that balance the rate reward and association-switching penalty in (24).

4) *DDQN Algorithm*: The UAV-BS association problem can be formulated as the maximization of the expected discounted cumulative reward over the time horizon, which is defined as $G = \sum_{n=1}^N \gamma_1^{n-1} r_n(s_n, a_n)$, where $0 \leq \gamma_1 \leq 1$ is a discount factor. The objective of the agent is to obtain the optimal decision policy π^* (i.e., selecting the optimal UAV-BS association $b(n)$) that maximizes G , which can be expressed as $\pi^* = \arg \max_{\pi} G$. To handle the time-varying candidate BS set and mitigate the ping-pong switching effects caused by satellite and UAV mobility, we employ a DDQN-based agent to learn the optimal policy π^* . In the DDQN framework, the optimal policy can be expressed as $\pi^* = \arg \max_a Q^{\pi^*}(s_n, a_n)$, where Q^{π^*} denotes the state-action value function, which is defined as $Q^*(s_n, a_n) = \mathbb{E}_{\pi} [\sum_{k=0}^{\infty} \gamma_1^k r_{n+k+1} \mid s_n = s, a_n = a]$.

At each decision step n , a deep neural network (DNN) parameterized by ω is employed to approximate the value function, while advanced network modules are also applicable [36]. Specifically, the evaluation network $Q(s, a; \omega)$ takes the current state s_n as input and outputs the Q-values corresponding to all possible actions $a \in \mathcal{A}$, which serve as the basis for action selection. To balance the trade-off between exploration and exploitation, we then adopt the ε -greedy policy

$$a_n = \begin{cases} \arg \max_{a \in \mathcal{A}} Q(s_n, a; \omega), & \text{with prob. } 1 - \varepsilon, \\ \text{randomly select } a \in \mathcal{A}, & \text{with prob. } \varepsilon, \end{cases} \quad (37)$$

where ε exponentially decays from $\varepsilon_{\text{init}}$ to $\varepsilon_{\text{final}}$, and remains fixed at $\varepsilon_{\text{final}}$ thereafter. After executing action a_n , the agent receives an immediate reward r_n and transitions to the next state s_{n+1} , where $\{s_n, a_n, r_n, s_{n+1}\}$ is stored in the replay buffer \mathcal{X}_1 , which can be seen in Fig. 2. During the network updating stage, a mini-batch of experiences $\mathcal{X}_{1,z}$ is randomly sampled from \mathcal{X}_1 . For each sampled experience, the target value is defined as the sum of the immediate reward and the discounted maximum Q-value of the next state, given by

$$y_n = r_n + \gamma_1 Q(s_{n+1}, \hat{a}_{n+1}; \omega'), \quad (38)$$

where $\hat{a}_{n+1} = \arg \max_{a \in \mathcal{A}} Q(s_{n+1}, a; \omega)$, and ω' denotes the parameters of the target network. The target network is employed solely for computing the target value y_n and does not participate in backpropagation to ensure training stability. The evaluation network is optimized by minimizing the mean square error (MSE) loss function

$$L(\omega) = \mathbb{E}_{\{s, a, r, s_{n+1}\} \in \mathcal{X}_{1,z}} [(y_n - Q(s_n, a_n; \omega))^2]. \quad (39)$$

The target network, evaluation network, and the loss function of the DDQN network can be observed in the lower-left part of Fig. 2. The network parameters are optimized using the Adam optimizer, given by [37]

$$\omega \leftarrow \text{Adam}(\nabla_{\omega} L(\omega), \eta_1), \quad (40)$$

where η_1 is the learning rate. To further enhance the training stability, the parameters of the training network are periodically copied to the target network every λ_U iterations by $\omega' \leftarrow \omega$. Unlike the basic DQN, our DDQN framework incorporates an adaptive exploration strategy, experience replay, and a dual-network architecture in Fig. 2, which not only alleviates Q-value overestimation and training oscillations in non-stationary environments but also significantly enhances the stability, convergence efficiency, and robustness of policy learning in highly dynamic SAGIN scenarios.

C. HDRL Lower-Level: CSAC for UAV Trajectory Control

Existing studies commonly discretize the continuous action space of UAV trajectory control, which not only introduces throughput loss but also depends on extensive heuristic rules for designing complex reward-penalty structures and numerous hyperparameters, thereby limiting their applicability in multi-constraint environments. Building on this, we propose a Lagrangian-based CSAC algorithm to optimize UAV trajectory in a continuous action space. The algorithm not only eliminates cumbersome reward and hyperparameter engineering but also naturally captures the nonlinear couplings between states and decision variables under multiple constraints.

1) *Lower-Level State Space*: As illustrated in Fig. 2, the top-level first generates and holds the UAV-BS association decision, upon which the lower-level produces the trajectory control actions, and the resulting new state is then fed back to the top-level to enable the update of the subsequent association decision in Section IV-A. For the 1-th lower-level time step corresponding to the m -th top-level time step, the UAV state $s_{m,1}$ consists of three components: (i) the UAV-BS association indicator b_m , (ii) the link rate $R_{m,1}$, and (iii) the UAV position vector $\mathbf{q}_{m,1} = (x_{m,1}, y_{m,1}, z_{m,1})$. Thus, the state of the 1-th lower-level time step corresponding to the m -th top-level time step can be expressed as

$$\mathbf{s}_{m,1} \triangleq [b_m, R_{m,1}, \mathbf{q}_{m,1}]^T. \quad (41)$$

2) *Lower-Level Action Space*: The action space of the agent is continuous, and each action represents the control of the UAV's trajectory direction at a time step. For each UAV, its new position in the next step is obtained by adding the current position and the action-induced displacement. The action $a_{m,1} = \vec{v}_{m,1}$ corresponds to the continuous selection

of the UAV's velocity control at each time step, where the velocity vector is treated as a continuous control variable in both direction and magnitude. Thus, the new UAV position $\mathbf{q}_{m,2}$ after taking the action can be expressed as

$$\mathbf{q}_{m,2} = \mathbf{q}_{m,1} + a_{m,1} V_{\max} \Delta t, \quad (42)$$

3) *Lower-Level Reward Function*: To guide the UAV to fly toward regions with better communication quality (24), the rate reward $r_{m,1}^{\text{rate}}$ is defined as

$$r_{m,1}^{\text{rate}}(s_{m,1}, a_{m,1}) = \frac{R_{m,2} - \min_E\{R\}}{\max_E\{R\} - \min_E\{R\}}, \quad (43)$$

where $R_{m,2}$ denotes the link rate after taking action $a_{m,1}$ and reaching the next state $s_{m,2}$. To encourage the agent to minimize the flight time (24), a goal-approaching reward $r_{m,1}^{\text{goal}}$ is defined as

$$r_{m,1}^{\text{goal}} = (D_{\max} - d_{m,2}) / (D_{\max} - D_{\min}), \quad (44)$$

where D_{\min} and D_{\max} denotes the initial distance between the UAV and the destination at the beginning of the mission and $d_{m,2}$ is the Euclidean distance from the UAV's current position to the target. Building on this, the future intrinsic reward function is formulated as

$$r_{m,1}(s_{m,1}, a_{m,1}) = \lambda_1 \cdot r_{m,1}^{\text{rate}} + \lambda_3 \cdot r_{m,1}^{\text{goal}}, \quad (45)$$

where λ_1 and λ_3 denote the weighting factors that balance the communication quality and flight-efficiency objectives in (24).

4) *Lower-Level Cost Function*: To ensure that the UAV satisfies both trajectory and QoS constraints during flight (26)(27)(28)(29), a cost function is introduced. To guide the UAV to fly toward regions with more stable and higher-quality communication links (27), the minimum rate requirement R_{req} represents the threshold of acceptable communication performance. Specifically, the QoS cost $c_{m,1}^{\text{qos}}$ is defined as

$$c_{m,1}^{\text{qos}} = (R_{m,2} - R_{\text{req}}) / R_{\text{req}}. \quad (46)$$

When $R_{m,2} \geq R_{\text{req}}$, the QoS cost becomes non-negative, representing a reward; otherwise, the QoS cost becomes a penalty. To constrain the UAV within the designated operational region in (26)(28)(29), a boundary penalty is imposed whenever the UAV's position violates this constraint

$$c_{m,1}^{\text{bnd}} = -\eta_{\text{bnd}} \mathbb{I}(\mathbf{q}_{m,2} \notin [\mathbf{q}_L, \mathbf{q}_U]), \quad (47)$$

where $\eta_{\text{bnd}} > 0$ is the boundary-penalty weight and $\mathbb{I}(\cdot)$ is an indicator function that equals one if the condition holds and zero otherwise. When the UAV remains within the feasible region, $c_{m,1}^{\text{bnd}} = 0$; otherwise, a negative penalty is applied. By designing cost functions that are in one-to-one correspondence with the constraints in problem \mathcal{P}_2 , we explicitly recast the original hard constraints as learnable cost signals, enabling the CSAC agent to adaptively balance optimization of the task objective and constraints during training.

5) *CSAC Algorithm*: In the lower-level of the HDRL framework, our objective is to derive, for each UAV, an optimal continuous control policy that maximizes its long-term cumulative return over the entire flight period while satisfying trajectory and QoS constraints. Specifically, the optimal policy can be formulated as

$$\begin{aligned} & \max_{\pi} \mathbb{E}_{\pi} \left[\sum_{n=0}^{\infty} \gamma_2^n r(s_n, a_n) \right] \\ & \text{s.t. } \mathbb{E}_{\pi} \left[\sum_{n=0}^{\infty} \gamma_2^n c_k(s_n, a_n) \right] \leq d_k, \forall k, \end{aligned} \quad (48)$$

where $r(s_n, a_n)$ denotes the instantaneous reward, $c_k(s_n, a_n)$ represents the cost function associated with the k -th constraint, and d_k is the corresponding tolerance threshold. To solve the above constrained optimization problem, we adopt the CSAC algorithm, which introduces a Lagrangian multiplier to explicitly embed the constraint terms into the objective function. This design enables the agent to maximize the expected cumulative reward while ensuring constraint satisfaction throughout the training process.

Specifically, we first define the soft state-action value function based on the policy π as

$$Q^{\pi}(s_n, a_n) = \mathbb{E}_{\pi} \left[\sum_n \left(r(s_n, a_n) - \sum_{i=1}^K \lambda_i c_i(s_n, a_n) + \alpha \mathcal{H}(\pi(\cdot | s_n)) \right) \right], \quad (49)$$

where $\lambda_i \geq 0$ denotes the Lagrange multiplier corresponding to the i -th constraint, α is the temperature coefficient, and $\mathcal{H}(\pi(\cdot | s_n))$ is the policy entropy term for actions at state s_n , where $\pi(\cdot | s_n)$ denotes the distribution of the action selection. $\mathcal{H}(\pi(\cdot | s_n))$ can be defined as $\mathcal{H}(\pi(\cdot | s)) = -\mathbb{E}_{a \sim \pi(\cdot | s)} [\log \pi(a | s)]$. By adopting the policy entropy term, SAC makes the probability distribution of continuous actions more uniform, leading to improved generalization capability and exploration ability.

The SAC framework consists of one actor network $\pi(\phi)$, which outputs a probabilistic action distribution, and four Q-critic networks that estimate the state-action values, including two evaluation networks $Q(\theta_1)$ and $Q(\theta_2)$ and their corresponding target networks $Q(\theta'_1)$ and $Q(\theta'_2)$ in Fig. 2. At initialization, $\theta'_1 \leftarrow \theta_1$ and $\theta'_2 \leftarrow \theta_2$. At each step, for each agent, the actor network $\pi(\phi)$ takes the state s_n as input and outputs the action distribution, including a mean scalar $\mu(s_n; \phi)$ and a standard deviation (STD) logarithm scalar $\hat{\sigma}(s_n; \phi)$. To control the range of STD, we clip $\hat{\sigma}(s_n; \phi)$ into $[-20, 2]$ and get $\hat{\sigma}_{\text{clip}}(s_n; \phi)$, then the STD can be obtained by $\sigma(s_n; \phi) = \exp(\hat{\sigma}_{\text{clip}}(s_n; \phi))$. SAC applies the reparameterization trick to sample the action, thereby reducing the variance of gradient estimation during back propagation [38]:

$$a = \Delta P \cdot \tanh [\mu(s_n; \phi) + \sigma(s_n; \phi) \cdot \xi], \quad (50)$$

where $\xi \sim \mathcal{N}(0, 1)$ is a Gaussian random number. The scaling coefficient ΔP and the $\tanh(\cdot)$ function are used to map the action value to the desired range. After executing the action a_n , the lower-level agent receives the reward r_n and next state s_{n+1} , and this experience $\{s_n, a_n, r_n, s_{n+1}\}$ is stored in the replay memory \mathcal{X}_2 . Subsequently, similar to the DDQN algorithm, SAC randomly samples a mini-batch of experience $\mathcal{X}_{2,z}$ from \mathcal{X}_2 to train the networks in Fig. 2.

The Q-critic networks are expected to estimate more accurate state-action values, so each Q-critic network (for $i = 1, 2$) can be trained by minimizing the loss function denoted as

$$L(\theta_i) = \mathbb{E}_{\mathcal{X}_{2,z}} \left[(Q(s_n, a_n; \theta_i) - y(r_n, s_{n+1}))^2 \right], \quad (51)$$

where the estimation target soft-Q value $y(r_n, s_{n+1})$ is given by $y(r_n, s_{n+1}) = r_n + \gamma_2 \left(\min_{i=1,2} Q(s_{n+1}, a_{n+1}; \theta_i) - \alpha \log \pi(a_{n+1} | s_{n+1}; \phi) \right)$, where a_{n+1} is the next action sampled from the actor network with input s_{n+1} , and $\pi(a_{n+1} | s_{n+1}; \phi)$ is the probability of a_{n+1} in the action distribution. Based on the gradients of (51), the parameters of the two evaluation Q-critic networks θ_1 and θ_2 can be updated similar to (40). Then, the parameters of the two target Q-critic networks θ'_1 and θ'_2 can be softly updated by

$$\theta'_i \leftarrow \tau \theta_i + (1 - \tau) \theta'_i, \quad i \in \{1, 2\}, \quad (52)$$

where $0 < \tau \ll 1$ is the soft updating factor. The actor network is expected to output actions with a larger composite metric including both Q-value and policy entropy. It can be trained by minimizing the loss function given by

$$L(\phi) = \mathbb{E}_{\{s_n\} \in \mathcal{X}_{2,m}} \left[\alpha \log \pi(\tilde{a}_n | s_n; \phi) - \min_{i=1,2} Q(s_n, \tilde{a}_n; \theta_i) \right], \quad (53)$$

where $\tilde{a}_n = \pi(s_n; \phi)$ is the action sampled from the current actor network with input s_n . Based on the gradients of (53), the parameters of the actor network ϕ can be updated similar to (40). The temperature α can be automatically updated by minimizing the loss function in Fig. 2:

$$L(\alpha) = \mathbb{E}_{\{s_n\} \in \mathcal{X}_{2,m}} \left[-\alpha (\mathcal{H}_{\text{target}} + \log \pi(\tilde{a}_n | s_n; \phi)) \right], \quad (54)$$

where the target entropy is set as $\mathcal{H}_{\text{target}} = -1$, i.e., the negative value of the action dimension. During each training iteration, in addition to updating the actor and critic networks, CSAC adaptively adjusts the Lagrange multipliers λ_i for each constraint according to

$$\lambda_i \leftarrow \left[\lambda_i + \eta_\lambda (\mathbb{E}[c_i(s_n, a_n)] - d_i) \right]_+, \quad (55)$$

where η_λ is the learning rate for the multipliers, and $[\cdot]_+$ denotes projection onto the nonnegative space. When the expected constraint cost $\mathbb{E}[c_i(s_n, a_n)]$ exceeds its limit d_i , the corresponding λ_i increases to impose a stronger penalty; otherwise, λ_i decreases gradually. In summary, the proposed CSAC algorithm explicitly incorporates Lagrangian multipliers to enable joint learning of continuous trajectory control and multiple constraints in (48), which maintains high exploration capability and training stability, while effectively avoiding cumbersome reward and hyperparameter engineering.

D. Overall HDRL Algorithm

The detailed pseudo-code of the proposed algorithm is provided in Algorithm 1 and explained as follows. Steps 1–2 initialize the network parameters and the initial states. Each training episode starts from the initial states of all UAVs. In Steps 4–13, the top-level DDQN agent in Section IV-B collects extrinsic transition samples and updates the top-level network parameters. In Steps 14–24, the lower-level CSAC agent in Section IV-C executes continuous trajectory control conditioned on the top-level decisions, collects intrinsic transition samples, and updates the lower-level network parameters. Finally, the top-level DDQN agent learns the optimal UAV-BS association policy, while the lower-level CSAC agent converges to the optimal UAV trajectory control policy, as

Algorithm 1 HDRL Algorithm

Require: $\varepsilon, \tau, \gamma_1, \gamma_2, \eta_1, \eta_2, \eta_\lambda$.

1: **Initialization:** Set $t = 0$ and initialize $\mathcal{X}_1, Q(\omega), Q(\omega')$ of DDQN agent and $\mathcal{X}_2, \pi(\phi), Q(\theta_1), Q(\theta_2)$ of CSAC agent.
2: Randomly initialize weights (ω, ω') and $(\theta_1, \theta_2, \alpha, \{\lambda_i\})$.
3: **for** each UAV **do**
4: **for** episode = 1 to M **do**
5: **for** each time step $n = 0, 1, \dots, N$ **do**
6: Observe s_n and execute a_n in (37).
7: Observe r_n and the next state s_{n+1} .
8: Store (s_n, a_n, r_n, s_{n+1}) into \mathcal{X}_1 .
9: Randomly sample a mini-batch $\mathcal{X}_{1,m}$ from \mathcal{X}_1 .
10: **for** each sample $\in \mathcal{X}_{1,m}$ **do**
11: Compute the target value in (38).
12: Update network parameters by (39) (40).
13: **end for**
14: **if** $n \bmod \lambda_U = 0$ **then**
15: Update target network parameters: $\omega' \leftarrow \omega$
16: **end if**
17: Observe $s_{n,1}$ and sample action $a_{n,1}$ by (50).
18: Observe $s_{n,2}, r_{n,1}$, and $c_{n,1}$.
19: Store $(s_{n,1}, a_{n,1}, r_{n,1}, s_{n,2}, c_{n,1})$ into \mathcal{X}_2 .
20: Randomly sample a mini-batch $\mathcal{X}_{2,m}$ from \mathcal{X}_2 .
21: **for** each sample $\in \mathcal{X}_{2,m}$ **do**
22: Compute the target value by (49).
23: Update critics by (51) and actor by (53).
24: Update the temperature by (54).
25: Update the multipliers by (55).
26: Update the target networks by (52).
27: **end for**
28: Update the top-level state by $s_{n+1} \leftarrow s_{n,2}$.
29: **end for**
30: **end for**
31: **end for**
Ensure: $\pi_T^*(a|s; \omega^*), \pi_L^*(a|s; \phi^*), Q_T^*(\omega^*), Q_L^*(\theta_1), Q_L^*(\theta_2), \alpha^*, \{\lambda_i^*\}$.

illustrated in Fig. 2. By hierarchically structuring the decision-making process and optimizing each level at its own temporal scale in Section IV-A, the top-level and lower-level decisions are effectively decoupled and learned at different temporal scales, which naturally reduces the dimensionality of the hybrid action space, lowers the computational complexity, and improves training stability.

V. NUMERICAL RESULTS

We consider an urban area of size 2 km \times 2 km with high-rise buildings, which represents a particularly challenging environment for coverage-aware UAV navigation. This is because Line-of-Sight (LoS) and Non-Line-of-Sight (NLoS) links, as well as the received signal strength, may vary frequently as the UAV moves through the area [25]. To accurately simulate the channel between the UAV and the BS in this environment, we first generate the positions and heights of buildings based on the statistical building model recommended by the International Telecommunication Union (ITU) [39]. This statistical building model has been widely adopted to evaluate the LoS probability of wireless links.

TABLE I
MAIN SYSTEM-LEVEL EXPERIMENT PARAMETERS

Parameter	Value
GN parameters	
BS frequency band	6.7 GHz
Bandwidth	1 MHz
Number of BS sites	3
Total number of cells	9
BS transmit power	46 dBm
BS antenna height	25 m
Antenna type	4 × 2 UPA
Antenna directivity	Directional
Electrical downtilt angle	10°
AN parameters	
BS frequency band	4.9 GHz
Bandwidth	1 MHz
Number of BS sites	3
Total number of cells	9
BS transmit power	46 dBm
BS antenna height	50 m
Antenna type	4 × 2 UPA
Antenna directivity	Directional
Electrical downtilt angle	-10°
SN parameters	
LEO orbital altitude	550 km
Number of LEO satellites	2
Satellite linear velocity	7.5 km/s
Carrier frequency	2.185 GHz
Bandwidth	1 MHz
Satellite transmit power	46 dBm
Beam pointing direction	[0, 0, -1]
Satellite antenna configuration	8 × 8 UPA
UAV parameters	
Min flight height	100 m
UAV speed	5, 10, 15, 20 m/s
UAV number	32
Antenna type	Omnidirectional, gain: 0 dBi

TABLE II
HDRL PARAMETERS

Parameter	Value
Top-Level: DDQN Parameters	
Number of neurons in hidden layers	128, 64
Exploration rate	0.5, 0.05
Replay memory and mini-batch size	50000, 128
Discounting factor	0.97
Target network updating period (steps)	200
Training network learning rate	0.0005
Lower-Level: CSAC Parameters	
Number of neurons in hidden layers	128, 64
Replay memory and mini-batch size	50000, 128
Discounting factor	0.99
Target critic network soft updating factor	0.005
Actor and critic network learning rate	0.0003

Unless otherwise specified in Table I, the remaining parameter settings are as follows:

1) *GN Parameters*: We consider a geographical area covered by three GN BS sites, each of which is sectorized into three sectors using the standard sectorization technique [32], resulting in a total of 9 GN cells. The three sectors are oriented toward azimuth angles of 0°, 120°, and 240°, respectively, yielding a directional radiation pattern for GN coverage [40].

2) *AN Parameters*: The ABS is a dedicated network designed for low-altitude coverage, which is deployed at a higher altitude and employs an electrical up tilt of 10° [33] so that the main beam points toward the low-altitude region.

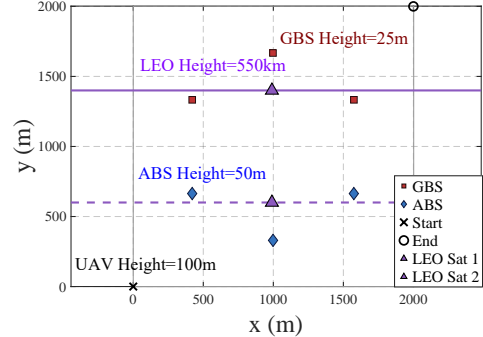


Fig. 3. Illustration of the SAGIN simulation scenario.

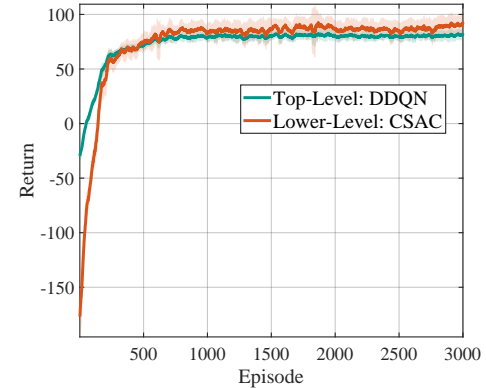


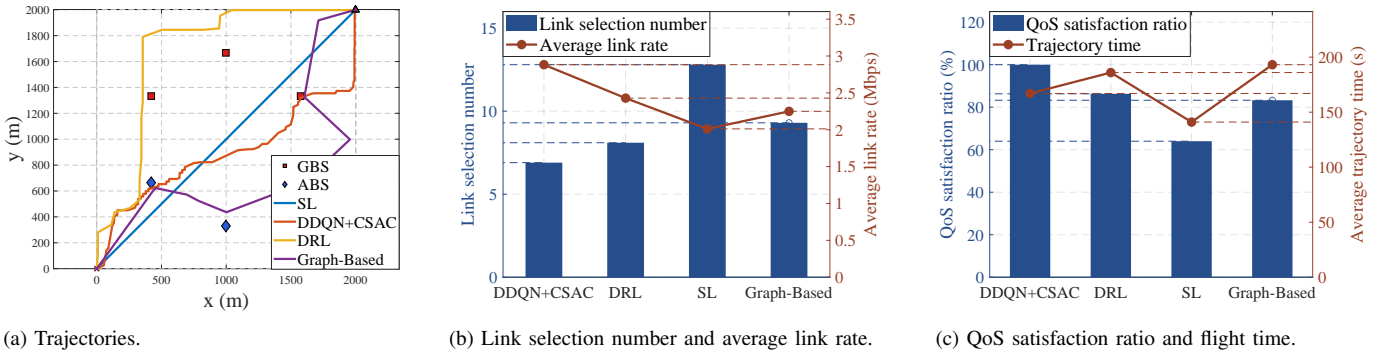
Fig. 4. Illustration of the HDRL training convergence performance.

The ABS operates in frequency bands dedicated to UAV communications [33].

3) *SN Parameters*: For the SN, two LEO satellites are considered. Both satellites move along the positive *x*-axis with a constant ground-projected velocity of 7.5 km/s [41]. Each satellite employs a fixed beam pointing vertically downward and is equipped with an 8 × 8 uniform planar array (UPA) [42].

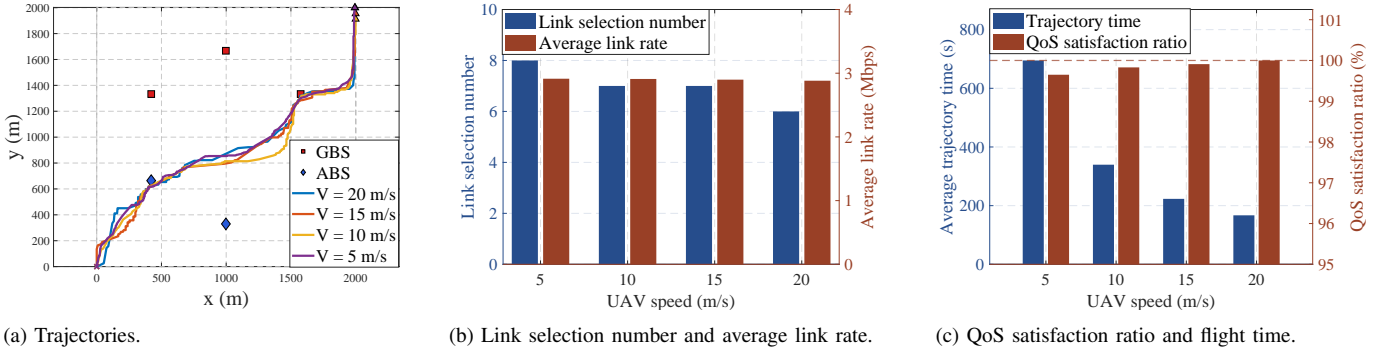
4) *Links*: For the AN-UAV and GN-UAV links, the building distribution generated earlier is first used to determine whether a LoS link exists between the UAV and each BS at a given UAV position. Subsequently, the path loss is calculated according to the 3GPP urban macro (UMa) model [43]. Small-scale fading is then superimposed: Rayleigh fading is adopted under NLoS conditions, while Rician fading with a Rician factor of 15 dB is applied under LoS conditions. For the SN-UAV link, the UAV generally maintains unobstructed visibility to the LEO satellite; thus, the channel is modeled using the 3GPP NTN urban LoS scenario [44], as illustrated in Fig. 3.

5) *HDRL Details*: Regarding the HDRL architecture [30], the top-level and lower-level agents are implemented as four-layer fully connected (FC) neural networks. Activation functions are set to rectified linear units (ReLUs), and the Adam optimizer [37] is adopted for gradient-based optimization in the networks. The maximum number of steps per episode is set to 300, and the HDRL training phase consists of 3000 episodes. After training, the simulation enters the testing stage, during which the HDRL networks are fixed and the agent executes optimal actions based on the observed states. Each testing phase consists of a single episode, and the detailed hyperparameter configurations are summarized in Table II.



(a) Trajectories.

Fig. 5. The performance with different benchmark methods.



(a) Trajectories.

Fig. 6. The performance with different UAV speeds.

A. Performance Comparison

To comprehensively evaluate the mobility management performance, we consider four metrics: the average link rate [21], the number of link selections [21], the QoS satisfaction ratio [45], and the flight time [25]. These metrics respectively characterize the throughput performance, link switching behavior, QoS guarantee, and flight efficiency of UAVs. Based on these metrics, we compare the proposed **DDQN+CSAC** algorithm with the following baseline methods:

- **Direct RL (DRL)** [26]: A baseline method that applies a DDQN algorithm by discretizing the continuous action space into a finite set of actions and selects the BS with the maximum SINR for connectivity.
- **Straight-Line Flight (SL)** [46]: A baseline method where the UAV flies directly from the start to the destination and connects to the BS with the highest RSRP.
- **Graph-Based** [24]: A baseline method that considers only the UAV's connectivity with GN and AN, and uses graph theory and convex optimization to obtain feasible and near-optimal solutions.

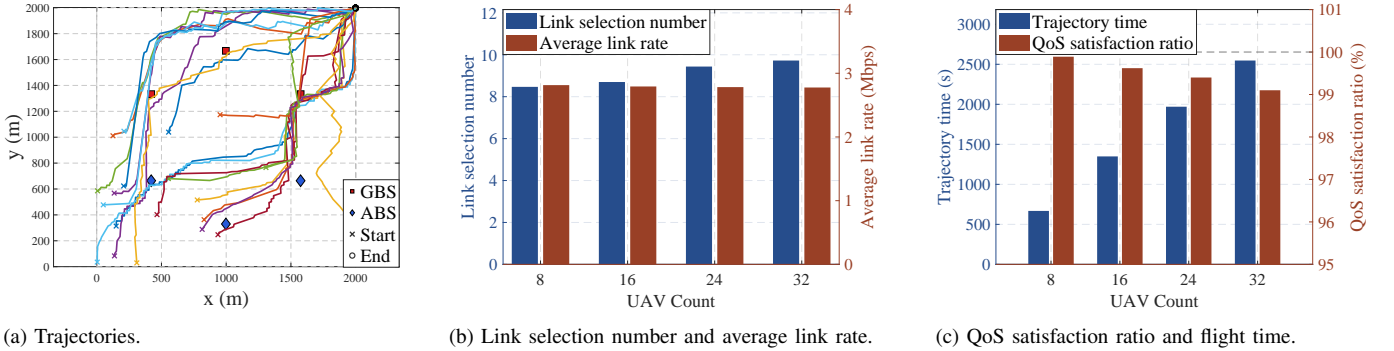
Fig. 4 illustrates the convergence behavior of the proposed **DDQN+CSAC** algorithm during training. It can be observed that the returns of both the top-level and lower-level agents gradually converge to stable values, indicating that the proposed algorithm achieves fast convergence, stable training, and effective learning.

Fig. 5a presents the UAV flight trajectories under different algorithms, while the performance of the four key metrics is illustrated in Fig. 5b and Fig. 5c. As shown in Fig. 5b, the proposed **DDQN+CSAC** algorithm achieves the best performance in terms of average link rate and the number of link selections, providing gains of 18.66% and 28.10% compared

with the **DRL** and **Graph-Based** schemes, respectively. This performance improvement arises because the **DRL** baseline discretizes the continuous action space, leading to quantization errors, whereas the proposed **DDQN+CSAC** framework decouples discrete and continuous decision variables in Section IV-A and employs CSAC in Section IV-C to effectively handle continuous trajectory control. Fig. 5c further shows that the proposed algorithm achieves the second-shortest flight time, only slightly longer than the **SL** scheme, while maintaining a 100% QoS satisfaction ratio throughout the entire flight. In contrast, the **DRL** and **SL** schemes achieve QoS satisfaction ratios of only 86.3% and 64%, respectively. This is because conventional **DRL** methods incorporate constraints into the reward function in an indirect manner, which cannot guarantee effective constraint satisfaction during execution. By contrast, the proposed **DDQN+CSAC** algorithm leverages CRL in Section IV-C to optimize long-term cumulative rewards while dynamically adjusting constraint weights in (48), thereby significantly enhancing QoS satisfaction.

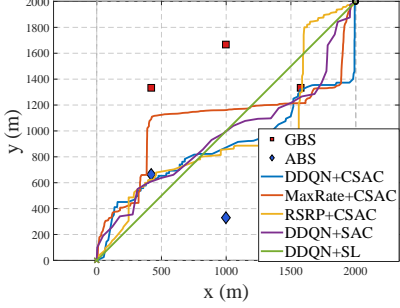
B. Robustness Testing

To further evaluate the robustness of the proposed **DDQN+CSAC** framework, we vary the UAV speed and the number of UAVs to assess its performance under different conditions. Fig. 6 illustrates the impact of different UAV velocities on the mobility management performance. As illustrated in Fig. 6b and 6c, the total flight time decreases and the number of link selections slightly reduces as the UAV speed increases. It can be seen that the proposed algorithm maintains high average link rates and QoS satisfaction ratios across different UAV speeds, demonstrating strong robustness. In Fig. 7, 32 UAVs are considered and they share the same destination location but start from different initial positions, and their corresponding



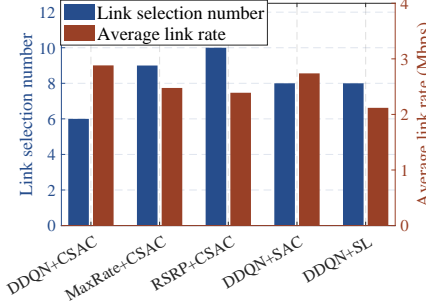
(a) Trajectories.

Fig. 7. The performance with different UAV numbers.



(a) Trajectories.

(b) Link selection number and average link rate.



(b) Link selection number and average link rate.

Fig. 8. The performance with different ablation experiments.

flight trajectories are depicted in Fig. 7a. In Fig. 7b and Fig. 7c, it can be observed that as the number of UAVs increases, the average number of link selections consistently remains within 8-10, the average link rate remains consistently high and stable, and the QoS satisfaction ratio remains above 99% across all cases. These results demonstrate that, empowered by the CTDE mechanism, the proposed algorithm exhibits strong adaptability and stability even in multi-UAV scenarios, thereby validating its reliability and robustness.

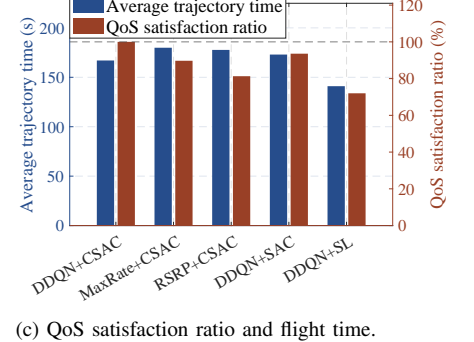
C. Ablation Experiment

To investigate how each level of HDRL respectively contributes to the performance gain, we perform an ablation experiment, where the four comparing algorithms are introduced. RSRP+CSAC and MaxRate+CSAC adopt greedy UAV-BS association strategies based on the maximum RSRP and maximum rate in the top-level, respectively, while DDQN+SAC and DDQN+SL employ a standard SAC algorithm and a straight-line flight strategy in the lower-level, with all remaining components identical to those of the proposed **DDQN+CSAC**. As shown in Fig. 8a, 8b, and 8c, both RSRP+CSAC and MaxRate+CSAC exhibit more frequent link selections and longer flight time, with their average link rates reduced by 14.09% and 17.08%, respectively, compared with the proposed **DDQN+CSAC**. This performance gap mainly arises from the DDQN long-term return learning mechanism in Section IV-B, which effectively balances instantaneous rate rewards and future cumulative gains, thereby reducing association-switching overhead and improving overall performance. In addition, although both consider QoS constraints in the lower-level, the coupling between their top- and lower-level policies hinders unified optimization, leading to inferior results, which further demonstrates the effectiveness of the proposed DDQN in the top-level in Section IV-B.

Besides, the results in Fig. 8b and 8c show that the proposed **DDQN+CSAC** achieves the fewest link selections while improving the average link rate by 5.24% and 36.04% compared with DDQN+SAC and DDQN+SL, respectively. These findings highlight the crucial role of trajectory optimization in enhancing communication performance, as jointly optimizing UAV trajectories enables better adaptation to link quality variations and significantly improves system throughput. The proposed **DDQN+CSAC** achieves the best performance in both flight time and QoS satisfaction rate. In contrast, DDQN+SAC treats the constraints merely as penalty terms in the reward function, forming a soft-constraint mechanism that cannot guarantee strict constraint satisfaction at every time step. By comparison, the proposed CRL framework in Section IV-C explicitly incorporates constraints into the optimization objective, enabling the agent to dynamically balance performance and constraint trade-offs during training, thereby achieving optimal performance while strictly satisfying all constraints, which further demonstrates the effectiveness of the proposed CSAC in the lower-level in Section IV-C.

VI. CONCLUSION

This paper investigated the joint link selection and trajectory optimization problem for high-mobility UAVs in SAGIN under multiple constraints. To reduce the computational complexity of traditional methods in highly dynamic environments, an HDRL framework was proposed, which decomposed the hybrid decision process into two levels: discrete UAV-BS association optimization and continuous trajectory control. The top-level employed a DDQN algorithm, while the lower-level adopted a Lagrangian-based CSAC algorithm, where both algorithms required only UAV signal measurements as input. Numerical results verified the effectiveness of the proposed HDRL framework, showing superior performance in system



throughput, link selection frequency, and convergence stability compared with benchmark schemes.

REFERENCES

- [1] W. Saad, M. Bennis, and M. Chen, "A vision of 6G wireless systems: Applications, trends, technologies, and open research problems," *IEEE Netw.*, vol. 34, no. 3, pp. 134–142, Jun. 2019.
- [2] S. Wu, Y. Wang *et al.*, "Distributed beamforming for multiple LEO satellites with imperfect delay and doppler compensations: Modeling and rate analysis," *IEEE Trans. Veh. Technol.*, vol. 74, no. 9, pp. 14 978–14 984, Sept. 2025.
- [3] Y. Wang, V. N. Ha *et al.*, "Statistical CSI-based distributed precoding design for OFDM-cooperative multi-satellite systems," *arXiv preprint arXiv:2505.08038*, May 2025.
- [4] P. Yang, Y. Xiao *et al.*, "6G wireless communications: Vision and potential techniques," *IEEE Netw.*, vol. 33, no. 4, pp. 70–75, Aug. 2019.
- [5] S. Dang, O. Amin *et al.*, "What should 6G be?" *Nature Electron.*, vol. 3, no. 1, pp. 20–29, Jan. 2020.
- [6] J. Xu, M. A. Kishk, and M. Alouini, "Space-air-ground-sea integrated networks: Modeling and coverage analysis," *IEEE Trans. Wireless Commun.*, vol. 22, no. 9, pp. 6298–6313, Sep. 2023.
- [7] H. Hou, Y. Wang *et al.*, "Joint beam alignment and doppler estimation for fast time-varying wideband mmWave channels," *IEEE Trans. Wireless Commun.*, vol. 23, no. 9, pp. 10 895–10 910, Sept. 2024.
- [8] X. Jing, F. Liu *et al.*, "ISAC from the sky: UAV trajectory design for joint communication and target localization," *IEEE Trans. Wireless Commun.*, vol. 23, no. 10, pp. 12 857–12 872, Oct. 2024.
- [9] S. Khosravi, H. Shokri-Ghadikolaei, and M. Petrova, "Learning-based handover in mobile millimeter-wave networks," *IEEE Trans. Cogn. Commun. Netw.*, vol. 7, no. 2, pp. 663–674, Jun. 2021.
- [10] A. Haghrah, M. P. Abdollahi *et al.*, "A survey on the handover management in 5G-NR cellular networks: Aspects, approaches, and challenges," *EURASIP J. Wireless Commun. Netw.*, vol. 2023, no. 1, p. 52, Jan. 2023.
- [11] S. Su, T. Chih, and S. Wu, "A novel handover process for mobility load balancing in LTE heterogeneous networks," in *Proc. IEEE Int. Conf. Ind. Cyber Phys. Syst. (ICPS)*. IEEE, May 2019, pp. 41–46.
- [12] T. Zhang, Y. Xu *et al.*, "Toward handover-free mobility management in FD-RAN: Architecture, challenges, and solutions," *IEEE Netw.*, vol. 38, no. 6, pp. 433–442, Nov./Dec. 2024.
- [13] S. Jaffry, R. Hussain *et al.*, "A comprehensive survey on moving networks," *IEEE Commun. Surv. Tutor.*, vol. 23, no. 1, pp. 110–136, First Quarter 2021.
- [14] T. M. Ho and K. Nguyen, "Joint server selection, cooperative offloading and handover in multi-access edge computing wireless network: A deep reinforcement learning approach," *IEEE Trans. Mobile Comput.*, vol. 21, no. 7, pp. 2421–2435, Jul. 2022.
- [15] R. Karmakar, G. Kaddoum, and S. Chattopadhyay, "Mobility management in 5G and beyond: A novel smart handover with adaptive time-to-trigger and hysteresis margin," *IEEE Trans. Mobile Comput.*, vol. 22, no. 10, pp. 5995–6010, Oct. 2023.
- [16] J. Yang, Z. Xiao *et al.*, "DQN-ALrM-based intelligent handover method for satellite-ground integrated network," *IEEE Trans. Cogn. Commun. Netw.*, vol. 9, no. 4, pp. 977–990, Dec. 2023.
- [17] Y. Kang, Y. Zhu *et al.*, "Joint server selection and handover design for satellite-based federated learning using mean-field evolutionary approach," *IEEE Trans. Netw. Sci. Eng.*, vol. 11, no. 2, pp. 1655–1667, Apr. 2023.
- [18] F. Wang, D. Jiang *et al.*, "Seamless handover in LEO-based non-terrestrial networks: Service continuity and optimization," *IEEE Trans. Commun.*, vol. 71, no. 2, pp. 1008–1023, Feb. 2022.
- [19] X. Xu, Z. Sun *et al.*, "Modeling and analyzing the cross-tier handover in heterogeneous networks," *IEEE Trans. Wireless Commun.*, vol. 16, no. 12, pp. 7859–7869, Dec. 2017.
- [20] Q. Liu, X. Li *et al.*, "User grouping-based beam handover scheme with load-balancing for LEO satellite networks," in *Proc. IEEE Glob. Commun. Conf. (GLOBECOM)*. IEEE, Dec. 2023, pp. 3965–3970.
- [21] F. Wang, S. Zhang *et al.*, "Sustainable UAV mobility support in integrated terrestrial and non-terrestrial networks," *IEEE Trans. Wireless Commun.*, vol. 23, no. 11, pp. 17 115–17 128, Nov. 2024.
- [22] S. Zhang, Y. Zeng, and R. Zhang, "Cellular-enabled UAV communication: A connectivity-constrained trajectory optimization perspective," *IEEE Trans. Commun.*, vol. 67, no. 3, pp. 2580–2604, Mar. 2018.
- [23] E. Bulut and I. Guvenc, "Trajectory optimization for cellular-connected UAVs with disconnectivity constraint," in *Proc. IEEE Int. Conf. Commun. Workshops (ICC Workshops)*. IEEE, May 2018, pp. 1–6.
- [24] S. Zhang and R. Zhang, "Trajectory design for cellular-connected UAV under outage duration constraint," in *Proc. IEEE Int. Conf. Commun. (ICC)*. IEEE, May 2019, pp. 1–6.
- [25] Y. Zeng, X. Xu *et al.*, "Simultaneous navigation and radio mapping for cellular-connected UAV with deep reinforcement learning," *IEEE Trans. Wireless Commun.*, vol. 20, no. 7, pp. 4205–4220, Jul. 2021.
- [26] C. Zhan and Y. Zeng, "Energy minimization for cellular-connected UAV: From optimization to deep reinforcement learning," *IEEE Trans. Wireless Commun.*, vol. 21, no. 7, pp. 5541–5555, Jul. 2022.
- [27] A. Madelkhanova, Z. Becvar, and T. Spyropoulos, "Optimization of cell individual offset for handover of flying base stations and users," *IEEE Trans. Wireless Commun.*, vol. 22, no. 5, pp. 3180–3193, May 2022.
- [28] R. Narmeen, Z. Becvar *et al.*, "Coordinated learning for handover management in 6G networks with transparent UAV relays," *IEEE Trans. Commun.*, vol. 73, no. 10, pp. 9553–9568, Oct. 2025.
- [29] X. Du, S. Zhang, and F. C. Lau, "Handover-aware trajectory optimization for cellular-connected UAV," *IEEE Wireless Commun. Lett.*, vol. 14, no. 7, pp. 1849–1853, Jul. 2025.
- [30] T. D. Kulkarni, K. Narasimhan *et al.*, "Hierarchical deep reinforcement learning: Integrating temporal abstraction and intrinsic motivation," in *Proc. Adv. Neural Inf. Process. Syst. (NeurIPS)*, vol. 29. NIPS, 2016.
- [31] M. Conti and S. Giordano, "Mobile ad hoc networking: Milestones, challenges, and new research directions," *IEEE Commun. Mag.*, vol. 52, no. 1, pp. 85–96, Jan. 2014.
- [32] 3GPP, "Study on 3D channel model for LTE," 3rd Generation Partnership Project (3GPP), Tech. Rep. 3GPP TR 36.873, V12.7.0, Dec. 2017, release 12.
- [33] S. Kim, M. Kim *et al.*, "Non-terrestrial networks for UAVs: Base station service provisioning schemes with antenna tilt," *IEEE Access*, vol. 10, pp. 41 537–41 550, Jan. 2022.
- [34] Y. Zeng, J. Lyu, and R. Zhang, "Cellular-connected UAV: Potential, challenges, and promising technologies," *IEEE Wireless Commun.*, vol. 26, no. 1, pp. 120–127, Feb. 2018.
- [35] 3GPP, "Solutions for NR to support non-terrestrial networks (NTN)," 3rd Generation Partnership Project (3GPP), Tech. Rep. 3GPP TR 38.821, Dec. 2019, version 16.2.0, Release 16.
- [36] Y. Wang, H. Hou *et al.*, "Toward unified AI models for MU-MIMO communications: A tensor equivariance framework," *IEEE Trans. Wireless Commun.*, vol. 24, no. 12, pp. 10 517–10 533, Dec. 2025.
- [37] D. P. Kingma and J. Ba, "Adam: A method for stochastic optimization," *arXiv preprint arXiv:1412.6980*, 2014.
- [38] T. Haarnoja, A. Zhou *et al.*, "Soft actor-critic algorithms and applications," *arXiv Preprint*, 2018, arXiv:1812.05905.
- [39] ITU-R, *Propagation Data and Prediction Methods Required for the Design of Terrestrial Broadband Radio Access Systems Operating in a Frequency Range from 3 to 60 GHz*, International Telecommunication Union (ITU) Recommendation ITU-R P.1410-5, Feb. 2012.
- [40] Y. Zeng, Q. Wu, and R. Zhang, "Accessing from the sky: A tutorial on UAV communications for 5G and beyond," *Proc. IEEE*, vol. 107, no. 12, pp. 2327–2375, Dec. 2019.
- [41] I. Leyva-Mayorga, B. Soret, and P. Popovski, "Inter-plane inter-satellite connectivity in dense LEO constellations," *IEEE Trans. Wireless Commun.*, vol. 20, no. 6, pp. 3430–3443, Jun. 2021.
- [42] L. You, X. Qiang *et al.*, "Integrated communications and localization for massive MIMO LEO satellite systems," *IEEE Trans. Wireless Commun.*, vol. 23, no. 9, pp. 11 061–11 075, Sep. 2024.
- [43] 3GPP, "Technical Specification Group Radio Access Network: Study on Enhanced LTE Support for Aerial Vehicles," 3rd Generation Partnership Project (3GPP), Technical Report 3GPP TR 36.777, Dec. 2017, version 15.0.0.
- [44] 3GPP, "Technical Specification Group Radio Access Network: Solutions for NR to Support Non-Terrestrial Networks (NTN)," 3rd Generation Partnership Project (3GPP), Technical Report 3GPP TR 38.821, Dec. 2019, version 16.0.0.
- [45] T. Zhang, J. Xue *et al.*, "Handover-free multi-connectivity mobility management for downlink FD-RAN: A hierarchical DRL-based approach," *IEEE Trans. Cogn. Commun. Netw.*, vol. 11, no. 2, pp. 1281–1296, Apr. 2025.
- [46] Y. Zhao, A. Xiao *et al.*, "Link quality-aware handover planning for space-aerial-terrestrial integrated networks," in *Proc. IEEE Global Communications Conference (GLOBECOM)*, Dec. 2023, pp. 1–6.